

OPTICAL ANISOTROPY OF InAs/GaSb BROKEN-GAP QUANTUM WELLS

A. A. Zakharova^{a,*}, *I. A. Semenikhin*^a, *K. A. Chao*^{b,c}

^a*Institute of Physics and Technology, Russian Academy of Sciences
117218, Moscow, Russia*

^b*Department of Physics, Lund University
S-22362, Lund, Sweden*

^c*Department of Physics, Chemistry, and Biology, Linköping University
S-58183, Linköping, Sweden*

Received July 13, 2011

We investigate in detail the optical anisotropy of absorption of linearly polarized light in InAs/GaSb quantum wells grown on GaSb along the [001] direction, which can be used as an active region of different laser structures. The energy level positions, the wave functions, the optical matrix elements, and the absorption coefficients are calculated using the eight-band $\mathbf{k} \cdot \mathbf{p}$ model and the Burt–Foreman envelope function theory. In these calculations, the Schrödinger and Poisson equations are solved self-consistently taking the lattice-mismatched strain into account. We find that a realistic Hamiltonian, which has the C_{2v} symmetry, results in considerable anisotropy of optical matrix elements for different directions of light polarization and different directions of the initial-state in-plane wave vector, including low-symmetry directions. We trace how the optical matrix elements and absorption are modified when spin-orbit interaction and important symmetry breaking mechanisms are taken into account (structural inversion asymmetry, bulk inversion asymmetry, and interface Hamiltonian). These mechanisms result in an almost 100 % anisotropy of the absorption coefficients as the light polarization vector rotates in the plane of the structure and in a plane normal to the interfaces.

1. INTRODUCTION

The knowledge on optical properties of broken-gap heterostructures with InAs/GaSb or similar quantum wells is of great importance because of intensive experimental investigations on the application of these structures for infrared laser generation. Cascade lasers with multiple quantum wells have been proposed [1] and realized experimentally [2–4]. The active region of these devices can contain more than ten stages consisting of InAs, GaSb, AlSb or other (for example, GaInSb or AlInSb) thin layers. The narrow-gap InAs and GaSb layers have two-dimensional electron and hole levels between which the optical transitions occur. The wide-gap AlSb (AlGaSb, AlInSb) tunneling barriers supply the transfer of the carriers through the structure to achieve the population inversion between the electron-like and hole-like levels and the laser generation. It was

shown that such a laser can operate at temperatures up to 100 K [4].

In cascade lasers, the first electron-like level in the InAs layer $1e$ is higher than the first heavy-hole-like level $1hh$ in the GaSb layer [5, 6]. The separation between them corresponds to the mid-infrared energy range for the emitted photons. However, the situation can be different for quantum wells with thicker InAs and GaSb layers. Because of an overlap of the InAs conduction band and the GaSb valence band, the $1e$ level can then be located below the $1hh$ level at the zone center (with the carrier in-plane wave vector $\mathbf{k}_{\parallel} = 0$) [5]. The $1e$ and $1hh$ levels anticross and hybridize for $\mathbf{k}_{\parallel} \neq 0$, which has been observed experimentally [7, 8] and studied theoretically [5, 9–11]. Laser generation in such thicker structures with hybridized electron–hole states has been also proposed [8]. In this case, the optical transitions exist between the states of the second electron-like subband $2e$ in the InAs layer and the lower hybridized states. These hybridizations

*E-mail: anna.alex.zakharova@gmail.com

can occur between two states (one electron state and one heavy-hole state or one electron state and one light-hole state). Also, three states (an electron state, a heavy-hole state, and a light-hole state) can hybridize [11].

The important feature of laser radiation is the polarization of the emitted light, which depends mainly on the optical anisotropy of broken-gap quantum wells. Theoretical study showed a strong dependence of the optical matrix elements and absorption coefficients on the direction of light polarization in type-I and type-II heterostructures [9, 10, 12–15]. This anisotropy is investigated here. We use the eight-band $\mathbf{k} \cdot \mathbf{p}$ method and the Burt–Foreman envelope function theory with the lowest conduction band states and the highest valence band states taken into account exactly and the other states treated perturbatively. The highest valence band includes the heavy-hole band, the light-hole band, and the split-off band whose states can mix and hybridize with each other and with the conduction band states. We solve the Schrödinger equation in the quantum well self-consistently to include the effects of charge accumulation at the contacts and the quantum well together with the realistic potential distribution, lattice-mismatched strain, and different symmetry-breaking mechanisms. We study the optical anisotropy of absorption coefficients for light linearly polarized along the growth direction [001] and in the plane of the structure along the [11] and $[1\bar{1}]$ directions. We also consider in detail the anisotropy of optical matrix elements for different directions of the initial state in-plane wave vector when the vector \mathbf{e} of light polarization is along [001], [11], or $[1\bar{1}]$ directions.

We outline the model used and the electron–hole hybridization in Sec. 2. The absorption of light polarized along the growth [001] direction (the z axis) is considered in Sec. 3 and in the plane of the structure, in Sec. 4. The optical anisotropy of the absorption coefficients is described in Sec. 5, and the conclusion is given in Sec. 6.

2. HYBRIDIZATION ELECTRON AND HOLE STATES

We study optical transitions in the InAs/GaSb quantum well sandwiched by two AlSb wide-gap barrier layers and two p -type GaSb contacts. In the structure with 10-nm InAs and 10-nm GaSb layers between 10-nm AlSb layers, the lowest electron-like level $1e$ at the zero in-plane wave vector lies below the highest hole level $1hh$. The acceptor concentration in contact

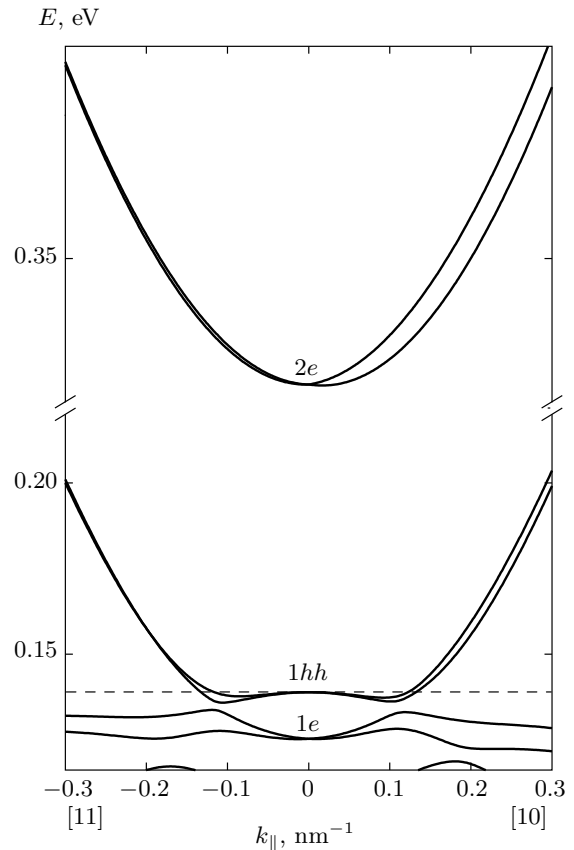


Fig. 1. Energy levels in the InAs/GaSb quantum well grown on GaSb along the [001] direction are shown by solid curves. The Fermi level is shown by a dashed line. The zero energy is set at the InAs conduction band edge near the AlSb/InAs heterojunction

layers is equal to 10^{18} cm^{-3} . The subband dispersions calculated self-consistently in this structure are shown in Fig. 1. We use the eight-band Hamiltonian for the region around the Γ point in the Brillouin zone,

$$\hat{H} = \begin{pmatrix} \hat{H}_4 & 0 \\ 0 & \hat{H}_4 \end{pmatrix} + \hat{H}_{so} + \hat{H}_\epsilon + \hat{H}_{\epsilon k} + \hat{H}_B + \hat{H}_k, \quad (1)$$

which is listed in Refs. [12, 13] for the set of basis functions

$$S \uparrow, X \uparrow, Y \uparrow, Z \uparrow, S \downarrow, X \downarrow, Y \downarrow, Z \downarrow.$$

The first block-diagonal matrix is the standard 8×8 Burt–Foreman Hamiltonian for structures made of zinc-blende materials, which neglects the spin-orbit interaction, strain effects, and symmetry-breaking mechanisms. The term \hat{H}_ϵ is the strain Hamiltonian independent of the momentum components k_i . The matrix \hat{H}_{so} describes the spin–orbit interaction of the

zeroth order in k_i and the matrix \hat{H}_{ek} is for the spin-orbit interaction in the strain Hamiltonian. This last term is nonzero due to the bulk inversion asymmetry (BIA). The quadratic-in- k_i matrix \hat{H}_B contains the Kane B -parameter. It represents the second BIA term in the total Hamiltonian (1). The term \hat{H}_k is the interface Hamiltonian (IH), which vanishes throughout the structure except at the interfaces. The interface Hamiltonian has a relativistic part (RIH) and a nonrelativistic part (NRIH). The Schrödinger equation for this Hamiltonian is a matrix equation for the eight-component envelope function Ψ , which is solved self-consistently with the Poisson equation.

The levels of the three subbands, $1e$, $1hh$, and $2e$, are spin-split due to the spin-orbit interaction, structural inversion asymmetry (SIA), BIA, and IH. These symmetry-breaking mechanisms also result in considerable anisotropy of dispersion curves for different directions of the quasiparticle in-plane wave vector. They change the selection rules for optical transitions for the transitions caused by light linearly polarized along the high-symmetry directions such as the $[001]$ growth direction, $[10]$ and $[01]$ directions in the plane of the quantum well if the initial state in-plane wave vector is also aligned with the high-symmetry directions ($[10]$ or $[01]$) [12, 13]. As a result, the optical matrix elements are nonzero for all the four possible transitions between two spin-split subbands $1hh$ and $2e$ (or $1e$ and $2e$). We first consider the anisotropy of the absorption of light polarized along the $[001]$ direction with respect to the \mathbf{k}_{\parallel} orientation and the resultant absorption coefficients for different thicknesses of the InAs layer and the GaSb layer of the quantum well. The hybridization of the $1hh$ and $1e$ subbands originating from the anti-crossing shown in Fig. 1 produces a substantial mixing of the electron and hole states, which also affects the optical properties.

3. ABSORPTION OF LIGHT POLARIZED ALONG THE GROWTH DIRECTION

We demonstrate the appearance of originally forbidden transitions and the strong angular dependence of the corresponding optical matrix elements M for the $1hh-2e$ absorption of light polarized along the $[001]$ direction, which we choose as the z axis. To distinguish the spin-split branches of each subband in the quantum well, we will assign the subscript “ a ” to the lower branch near the zone center and the subscript “ b ” to the higher one. We present our results for the normal-

ized value of the optical matrix element, which is given by

$$|M_0|^2 \equiv |\hbar M / \sqrt{2m}|^2, \quad (2)$$

where m is the free electron mass. The matrix element M is calculated with the transition operator defined as

$$\mathbf{e} \cdot \hat{\mathbf{v}} = \frac{\mathbf{e}}{\hbar} \cdot \frac{\partial \hat{H}}{\partial \hat{\mathbf{k}}}, \quad (3)$$

where $\hat{\mathbf{v}}$ is the velocity operator.

In Fig. 2, we show the squared absolute values of normalized optical matrix elements $|M_0|^2$ for the $1hh_b-2e_a$, $1hh_a-2e_b$, $1hh_a-2e_a$, and $1hh_b-2e_b$ transitions versus the angle ϕ between the $[10]$ direction, which we choose as the x axis, and \mathbf{k}_{\parallel} . We set the value of the in-plane wave vector equal to 0.1 nm^{-1} .

The plots in Fig. 2a have been obtained neglecting the IH, and the plots in Fig. 2b have been obtained neglecting the NRIH only. The matrix elements in Fig. 1c correspond to the total Hamiltonian. The four types of transitions are permitted and their intensities are substantial in each panel in Fig. 2. On the other hand, the intensities of only two types of spin-preserving transitions are considerable if both the BIA and IH are disregarded. Then the spin-flip transitions are forbidden for \mathbf{k}_{\parallel} along some high-symmetry direction such as $[10]$, $[11]$. If \mathbf{k}_{\parallel} is along a low-symmetry direction, for example, $[12]$, then the intensity of the warping-induced spin-flip processes is negligibly small. Also, the anisotropy of optical matrix elements with respect to different directions of \mathbf{k}_{\parallel} is very weak. The BIA, RIH, and NRIH produce strong qualitative changes of the angular dependences of the optical matrix elements. This is because of the mixing of spin-up and spin-down states due to symmetry-breaking terms in the Hamiltonian and the transition operator.

The absorption coefficient $J(\hbar\omega)$ of linearly polarized light with photon energy $\hbar\omega$ for the InAs/GaSb quantum wells with a 10-nm InAs layer and a 10-nm GaSb layer is shown in Fig. 3 with the solid curve. We have used the equation for the absorption coefficient given in Ref. [16],

$$J(\hbar\omega) = \frac{2\hbar\omega}{\pi n c E_0^2} \int dk_x dk_y f_t (1 - f_s) W_{st}(\omega), \quad (4)$$

where $\hbar\omega$ is the transition energy, c is the speed of light, n is the refractive index, E_0 is the electric field amplitude in the wave, $W_{st}(\omega)$ is the transition rate between the states of the s and t subbands, and $f_{t,s}$ are the respective occupations of the initial and final states.

The two peaks in this curve are due to the $1hh-2e_a$ and $1hh-2e_b$ transitions around $k_{\parallel} = 0.1 \text{ nm}^{-1}$, where

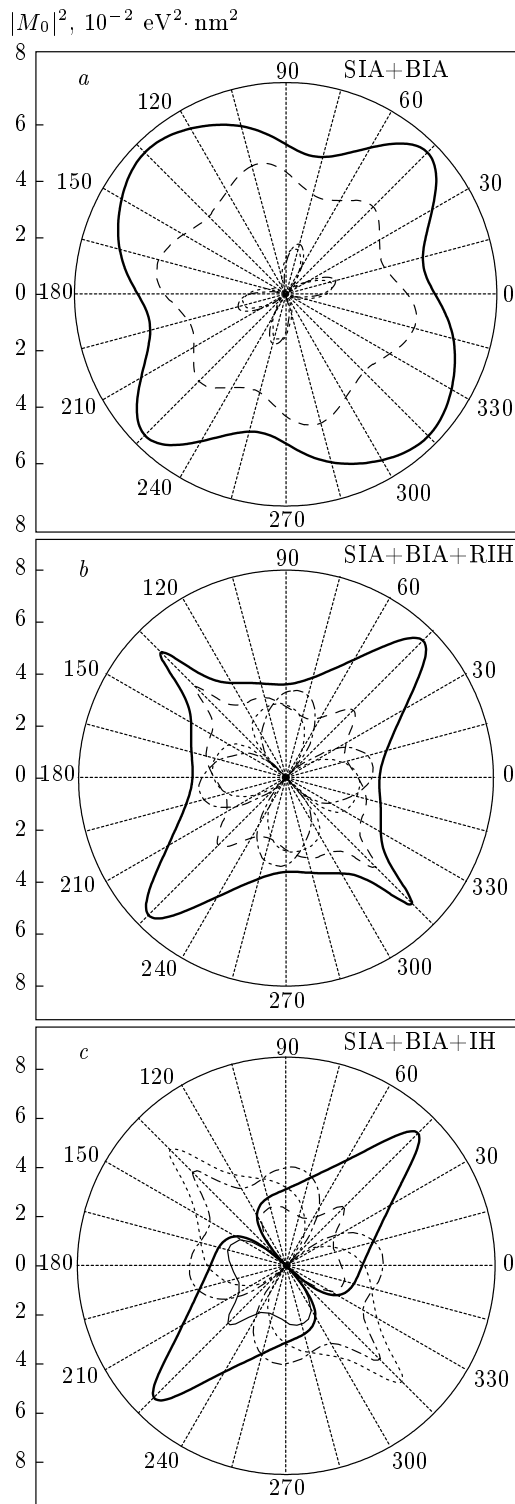


Fig. 2. The absolute value squared of the normalized optical matrix element $|M_0|^2$ versus the angle ϕ for the $1hh-2e$ transitions with $k_{\parallel} = 0.1 \text{ nm}^{-1}$. The solid, dashed, dotted, and dash-dotted curves respectively correspond to the $1hh_b-2e_a$, $1hh_a-2e_b$, $1hh_a-2e_a$, and $1hh_b-2e_b$ transitions. Light is polarized along the $[001]$ direction

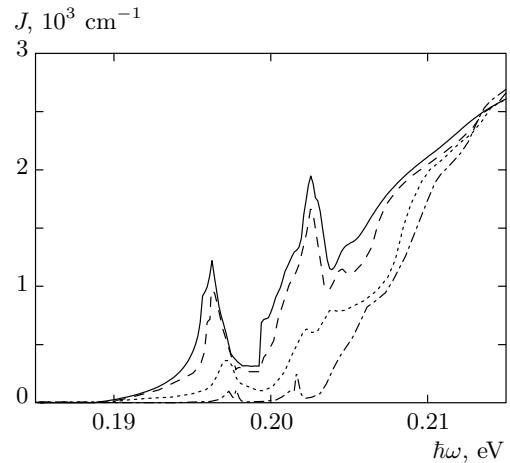


Fig. 3. Absorption coefficient for the InAs/GaSb quantum well with a 10-nm InAs layer and a 10-nm GaSb layer is shown by the solid curve, obtained taking the SIA, BIA, and IH into account. The dashed curve was calculated with the NRIH neglected, the dotted curve was found with the total IH neglected, and dash-dotted curve was obtained with both the BIA and IH neglected. Light is polarized along the $[001]$ direction

the $1hh$ states are occupied by electrons. The different energies of these transitions are mainly due to the spin splitting of the $2e$ states at $k_{\parallel} = 0.1 \text{ nm}^{-1}$, because of the small spin splitting of the $1hh$ states. Hence, the energy separation of two peaks in the solid curve reflects the spin splitting of the $2e$ subband. Dashed and dotted curves in Fig. 3 were respectively calculated with the NRIH and the total IH neglected. The absorption plotted with the dash-dotted curve was derived disregarding the BIA and IH. In the latter case, the two peaks of absorption in the solid curve vanish, because the spin-flip transitions between the states of the $1hh$ and $2e$ subbands are almost forbidden.

We now consider how our results change with the InAs and GaSb layer thickness variation. In Fig. 4, we show the absorption coefficients of light polarized along the growth direction $[001]$ for the structure with a 10.5-nm InAs layer and a 10.5-nm GaSb layer (solid curve), and for the structure with a 9.5-nm InAs layer and 9.5-nm GaSb layer (dashed curve). The first and third absorption peaks for each InAs/GaSb quantum well correspond to the two absorption peaks resulting from the $1hh-2e$ transitions, as our calculations showed. The separation between the peaks gives the characteristic value of spin splitting of the $2e$ levels. This spin splitting is about 4 meV for the structure with the InAs and GaSb layer thickness 9.5 nm, 6 meV

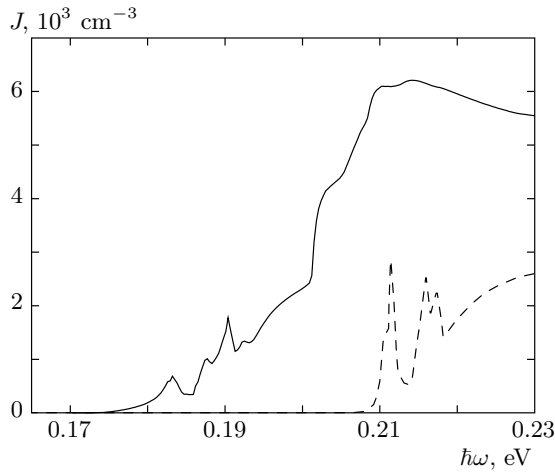


Fig. 4. Absorption coefficients for the InAs/GaSb quantum wells with 10.5-nm InAs (GaSb) layers (solid curve) and 9.5-nm InAs (GaSb) layers (dashed curve). Light is polarized along the [001] direction

if this thickness is 10 nm, and 8 meV if this thickness is 10.5 nm. We note that only the $1hh-2e$ and $1e-2e$ transitions contribute to the absorption in the energy interval considered for the dashed curve, while the solid curve was obtained also taking the contributions from the $2hh-2e$ and $1lh-2e$ transitions into account. The absorption peaks caused by the $1hh-2e$ transitions grow as the layer thickness decreases, because of the increasing hybridization of $1e$ and $1hh$ states, which become closer to each other in real space. Such a hybridization results in increased intensities of the originally forbidden spin-flip transitions from the states of the $1hh$ subband.

4. ABSORPTION OF LIGHT POLARIZED IN THE PLANE OF THE STRUCTURE

The optical matrix elements exhibit substantial anisotropy with respect to different directions of light polarizations in the plane of the quantum well $\mathbf{e} = \mathbf{e}_1$ and $\mathbf{e} = \mathbf{e}_2$. Figures 5 show the plots of the absolute values squared of normalized optical matrix elements $|M_0|^2$ for the $1hh_b-2e_a$, $1hh_a-2e_b$, $1hh_a-2e_a$, and $1hh_b-2e_b$ transitions versus the angle ϕ for \mathbf{e}_1 along the [11] direction and \mathbf{e}_2 along the $[1\bar{1}]$ direction, calculated with the BIA, RIH, NRIH symmetry-breaking mechanisms taken into account. The results for $\mathbf{e} = \mathbf{e}_1$ obtained with BIA and IH neglected turn into those for $\mathbf{e} = \mathbf{e}_2$ by rotation through the angle $\pi/2$. Then there is no lateral optical anisotropy of the absorption coefficients, but there exists a considerable anisotropy

of optical matrix elements investigated previously [9]. This symmetry breaks when we add BIA in the upper panels, BIA and the relativistic IH in the middle panels, and BIA and the total IH in the lower panels. The symmetry of the system is C_{2v} due to the SIA and BIA or SIA and IH. In passing from the upper panel to the lower panel in each figure, the optical matrix elements exhibit unusual qualitative changes. The BIA and IH reduce the mean values of M for light polarized along the [11] direction and enhances them for light polarization along the $[1\bar{1}]$ direction, resulting in a considerable anisotropy of the absorption coefficients shown in Fig. 6. Panels *a* and *b* in this figure are for the absorption coefficient J_1 and J_2 corresponding to the optical matrix elements in Figs. 5*a* and 5*b*. Many peaks in each panel in Fig. 6 originate from the overlap of eight absorption curves for the transitions between the spin-split hybridized $1e-1hh$ states and the spin-split $2e$ states.

5. OPTICAL ANISOTROPY OF ABSORPTION COEFFICIENTS

A considerable difference between the absorption coefficients $J_1(\hbar\omega)$ and $J_2(\hbar\omega)$ for different light polarizations $\mathbf{e} = \mathbf{e}_1$ and $\mathbf{e} = \mathbf{e}_2$, can be expressed by a value of polarization λ defined as

$$\lambda = \frac{J_2(\hbar\omega) - J_1(\hbar\omega)}{J_2(\hbar\omega) + J_1(\hbar\omega)}. \quad (5)$$

We show the calculated polarization versus the transition energy in Fig. 7. When light is polarized along the growth direction, the absorption coefficient is much higher than those for light polarized in the plane of the structure. This characteristic feature originates from the symmetry of wave functions of the electron and hole states near the zone center. With the mixing of the s -type conduction band wave functions and p -type valence band wave functions neglected, only the transitions from the electron-like states activated by light with \mathbf{e} along the growth direction are permitted. At $\mathbf{k}_{\parallel} \neq 0$, the s -type and p -type wave functions mix, resulting in the substantial absorption when the polarization vector \mathbf{e} lies in the plane of the structure. Then the spin-orbit interaction, SIA, and warping give rise to the anisotropy of optical matrix elements with respect to different directions of \mathbf{k}_{\parallel} , but not to the anisotropy of the absorption coefficients with the rotation of \mathbf{e} in the plane of the structure.

The BIA, RIH, and NRIH create the lateral optical anisotropy of absorption [12–14, 17, 18]. The main

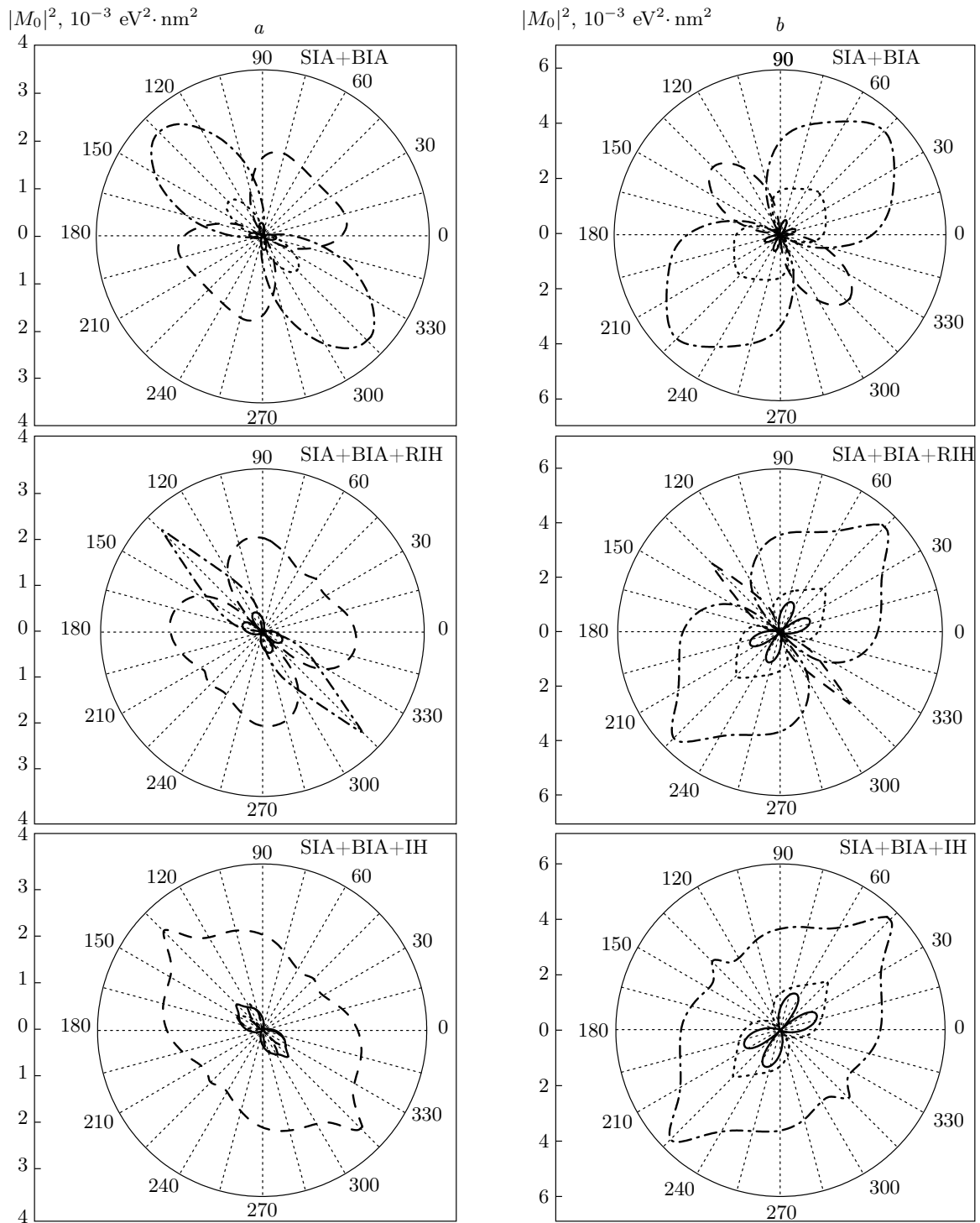


Fig. 5. The absolute value squared of the normalized optical matrix element $|M_0|^2$ versus the angle ϕ for the $1hh-2e$ transitions with $k_{||} = 0.1 \text{ nm}^{-1}$. The solid, dashed, dotted, and dash-dotted curves correspond to the $1hh_b-2e_a$, $1hh_a-2e_b$, $1hh_a-2e_a$, and $1hh_b-2e_b$ transitions. Light is polarized along the $[11]$ (a) and $[\bar{1}\bar{1}]$ (b) directions

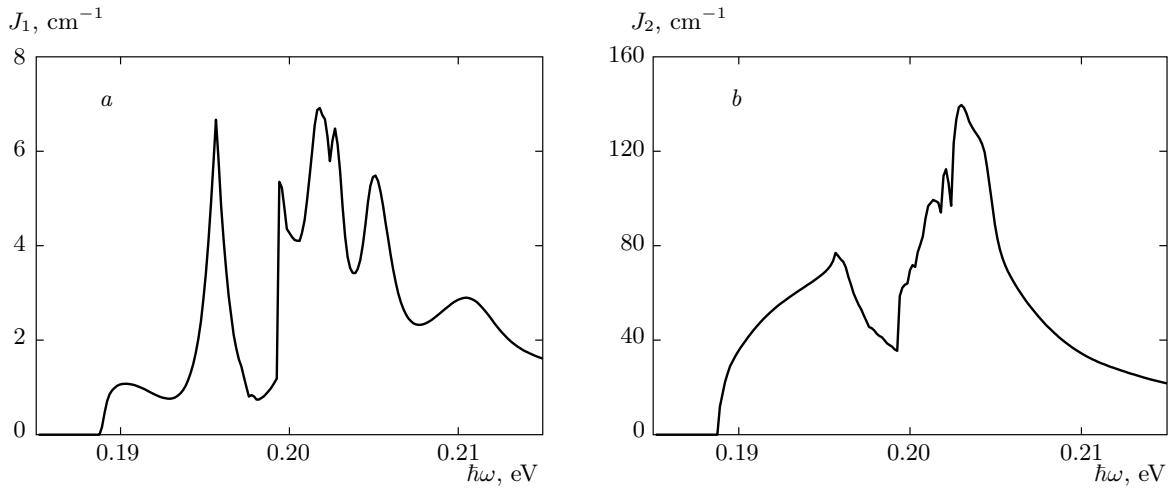


Fig. 6. Absorption coefficients for the InAs/GaSb quantum well with a 10-nm InAs layer and a 10-nm GaSb layer. Light is polarized along the [11] (a) and $[1\bar{1}]$ (b)

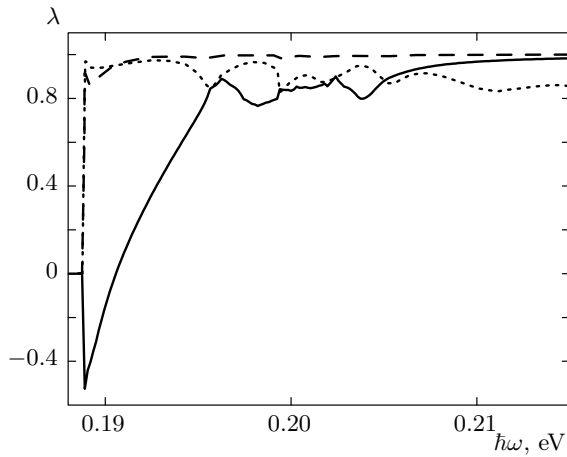


Fig. 7. Optical anisotropy for the quantum well with a 10-nm InAs layer and a 10-nm GaSb layer calculated with the total Hamiltonian. The solid curve represents the values of λ obtained when we align \mathbf{e}_2 with the [001] direction and \mathbf{e}_1 with the $[1\bar{1}]$ direction. The dashed curve corresponds to \mathbf{e}_2 along the [001] direction and \mathbf{e}_1 along the [11] direction. Finally, when \mathbf{e}_2 is along the $[1\bar{1}]$ direction and \mathbf{e}_1 is along the [11] direction, the results are represented by the dotted curve

contribution to this effect in the considered broken-gap quantum wells comes from the BIA terms in the transition operator proportional to the material-dependent Kane B -parameter [12]. These terms give the interface-localized contribution to the optical matrix elements and considerably modify the dependences of absorption

on the transition energy. As a result, the obtained values of λ represented by the dotted curve in Fig. 7 are very close to 100 % if the light polarization vector lies in the plane of the structure. If \mathbf{e}_2 is along the growth direction, λ is also close to 100 % for \mathbf{e}_1 along the [11] direction.

6. SUMMARY

In summary, we have investigated the strong optical anisotropy of broken-gap quantum wells of the InAs/GaSb type with respect to different directions of the light polarization vector \mathbf{e} and to different directions of the initial-state in-plane wave vector \mathbf{k}_{\parallel} . The optical transitions between the hybridized electron-hole states $1e-1hh$ and the states in the upper electron-like subband $2e$ have been considered. The dependences of $|M|^2$ on the angle between the [10] direction in the plane of the structure and \mathbf{k}_{\parallel} exhibit unusual qualitative changes when the BIA and IH are taken into account, which activates the transitions that were almost forbidden originally. These transitions considerably enhance the absorption of light polarized along the [001] growth direction and the $[1\bar{1}]$ direction in the plane of the structure. However, the absorption decreases for \mathbf{e} along the [11] direction. This gives rise to a nearly 100 % optical anisotropy of the absorption coefficients when \mathbf{e} rotates in the plane of the quantum well or in the plane perpendicular to it.

This work was financially supported by the Russian Foundation for Basic Research (grant No. 07-02-00680-a).

REFERENCES

1. R. Q. Yang, *Superlatt. Microstruct.* **17**, 77 (1995).
2. H. C. Liu and A. J. SpringThorpe, *Phys. Rev. B* **61**, 15629 (2000).
3. Rui Q. Yang, J. L. Bradshaw, J. D. Bruno et al., *Appl. Phys. Lett.* **81**, 397 (2002).
4. C. L. Canedy, W. W. Bewley, J. R. Lindle et al., *Appl. Phys. Lett.* **88**, 161103 (2006).
5. M. Altarelli, *Phys. Rev. B* **28**, 842 (1983).
6. X. Cartoixa, D. Z.-Y. Ting, and T. C. McGill, *Phys. Rev. B* **68**, 235319 (2003).
7. A. J. L. Poulter, M. Lakrimi, R. J. Nicholas et al., *Phys. Rev. B* **60**, 1884 (1999).
8. T. P. Marlow, L. J. Cooper, D. D. Arnone et al., *Phys. Rev. Lett.* **82**, 2362 (1999).
9. E. Halvorsen, Y. Galperin, and K. A. Chao, *Phys. Rev. B* **61**, 16743 (2000).
10. R. Magri, L. W. Wang, A. Zunger et al., *Phys. Rev. B* **61**, 10235 (2000).
11. A. Zakharova, S. T. Yen, and K. A. Chao, *Phys. Rev. B* **64**, 235332 (2001).
12. I. Semenikhin, A. Zakharova, K. Nilsson, and K. A. Chao, *Phys. Rev. B* **76**, 035335 (2007).
13. I. Semenikhin, A. Zakharova, and K. A. Chao, *Phys. Rev. B* **77**, 113307 (2008).
14. A. Zakharova, I. Semenikhin, and K. A. Chao, *Semicond. Sci. Technol.* **23**, 125044 (2008).
15. Paulo V. Santos, P. Etchegoin, M. Cardona et al., *Phys. Rev. B* **50**, 8746 (1994).
16. R. Winkler, M. Merkler, T. Darnhofer, and U. Rössler, *Phys. Rev. B* **53**, 10858 (1996).
17. L. W. Wang, S. H. Wei, T. Mattila et al., *Phys. Rev. B* **60**, 5590 (1999).
18. Bradley A. Foreman, *Phys. Rev. Lett.* **86**, 2641 (2001).